11th International Symposium on Magnetic Bearings
August 26-29, Nara, Japan

A SUPERCRITICAL 250 kW INDUSTRIAL AIR COMPRESSOR PROTOTYPE

Erkki Lantto, Ville Tommila
High Speed Tech Oy Ltd, Espoo 02150, Finland
erkki.lantto@absgroup.com, ville.tommila@absgroup.com

ABSTRACT
This paper presents the active magnetic bearing control system synthesis and practical rotor dynamic experiences with a supercritical 250 kW turbo compressor. First, the physical boundary conditions of passing the first bending critical speed and feasible bearing characteristics near the critical speed are considered. Then, the control system is synthesized and analyzed using complex formulation. A synchronous response controller is added in parallel with the position controller in order to achieve the preferred bearing characteristics. Finally, measured performance of the control system when passing the critical speed with a real life compressor is presented

INTRODUCTION
High Speed Tech Oy Ltd. (HST) is a manufacturer of high speed turbo compressors equipped with active magnetic bearings (AMB). Up until today, HST has delivered approximately 900 compressors in the power range from 50 kW to 250 kW. A few years ago a product prototype utilizing a squirrel cage induction motor was built and tested. Due to the flexible structure of the motor part of the rotor, a supercritical construction was necessary.

This paper concentrates on aspects of controlling the unbalance response near the first bending critical speed. It is a well known fact that, in the unbalance response point of view, a speed independent position controller can not be optimal in a wide speed range. Requirements of stability prevent this [9]. Too high unbalance leads to amplifier saturation at high speeds causing degradation of the bearing dynamics and even instability. A common solution to the saturation problem is to add a rotation synchronized narrow band filter in series with the position controller in order to eliminate the rotational synchronous control current vibration [4], [7] and [9]. Near a bending critical speed this approach can not be used since bearing forces are required to limit the vibration amplitudes. One option near the critical speed is to use whirling cancellation. This may be feasible in some cases, but generally it gives acceptable response only in a narrow speed range near the critical speed. One way is to formulate the unbalance response treatment to a mathematical optimization problem [8]. Naturally, such a general approach is capable of handling a variety of vibration control problems including passing the critical speeds. In [5] a rotation synchronized filter is attached in parallel with the position controller so that a narrow band phase lead section is obtained. In that solution, the gain of the total controller at the critical speed is non zero but finite and phase angle is adjusted so that the bearings acts as a pure damper at the rotation frequency [6]. This is also our conclusion of how the bearing characteristics should look like in the vicinity of a bending critical speed. The control circuit is generalized to allow exact adjustment of the general MIMO response to the preferred value in a straightforward way. Also the force cancellation is achieved as a special case. We call our approach synchronous response control (SRC).

THE MACHINE AND THE COMPONENTS
The compressor is shown in Figure 1. The application is a water treatment compressor with maximum electric input power of 250 kW and maximum speed of 320 Hz. The motor is a 2-pole squirrel cage induction motor.

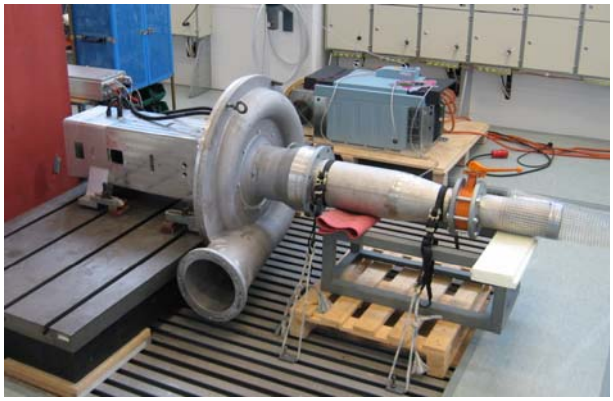

FIGURE 1: The compressor in the laboratory test stand.

Rotordynamic model
The rotor modeling was done using axi-symmetrical 3D finite elements [3]. Triangular isoparametric quadratic elements were used, see Figure 2.

Low order complex equation of motion [3], Equation 1, was constructed by modal reduction. Five first bending modes were included. The acceleration terms were omitted, since they have no practical effect on the present study. In a complex quantity, for example displacement or force, the real part presents the value in X direction and the imaginary part the value in Y direction.

$$\boldsymbol{M}_{\text{rotor}}\ddot{\boldsymbol{q}} - i\Omega\boldsymbol{G}_{\text{rotor}}\dot{\boldsymbol{q}} + \boldsymbol{K}_{\text{rotor}}\boldsymbol{q} = \boldsymbol{B}_{\text{B}}\boldsymbol{f}_{\text{B}} + \Omega^2 e^{i\beta}\boldsymbol{U}$$
$$\boldsymbol{p}_{\text{S}} = \boldsymbol{B}_{\text{S}}^{\text{T}}\boldsymbol{q} \qquad (1)$$

where $\boldsymbol{q}$ is modal degree of freedom vector, $\boldsymbol{p}_{\text{S}}$ is displacement in the sensor locations, $\boldsymbol{f}_{\text{B}}$, bearing force, $\boldsymbol{U}$ unbalance vector, β is rotation angle and Ω rotational speed, $\Omega = \dot{\beta}$. Modes 1,3,4,...,7 were scaled so that unity amplitude gives maximum displacement of 1 m and the rigid tilting mode, mode 2, so that a unity amplitude modal degree of freedom means one radian turning of the rotor. A constant unbalance vector, $\boldsymbol{U}_{\text{tst}}$, was used in all the simulations. Numerical values of the model matrices and $\boldsymbol{U}_{\text{tst}}$ are given in Appendix A.

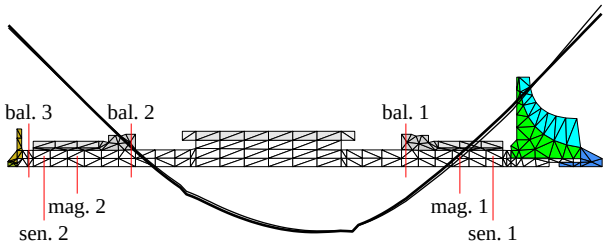

FIGURE 2: The FE mesh and locations of the sensors, magnets and balancing planes. The first free-free bending mode shape at critical speed is drawn with bold curve and at zero speed with thin curve.

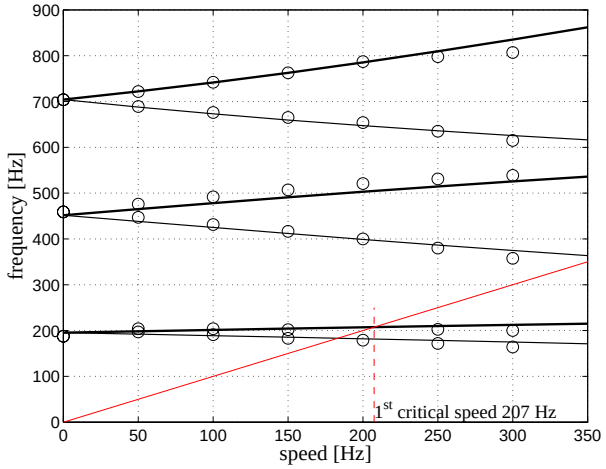

FIGURE 3: Campbell diagram. Calculated free-free natural frequencies are drawn with solid curves and measured frequencies are drawn with circles.

Magnetic bearings

The radial magnetic bearings were 8-pole, heteropolar bearings [9]. The key parameters of the radial AMB system are listed in Table 1. The controller used was MBC-12, a fully digital magnetic bearing controller made by HST. The dynamics of the position sensor anti alias filter, control delay and the power amplifier response are described by a transfer function $g(s)$.

TABLE 1: Parameters of the radial AMB system.

Item	Symbol	Value	Unit
Sampling interval	T	102.4	μs
Current stiffness	k_{I}	340	N/A
Position stiffness	k_{P}	2.3	MN/m
Coil inductance		42	mH
DC-link voltage	$U_{\max}$	150	V
Maximum current	$I_{\max}$	12	A
Load capacity, 0 Hz	F_{Bmax}	1300	N
Load capacity, 207 Hz	(ω)	800	N
Radial bearing air gap	δ	0.55	mm

Forces acting to the rotating part

In rotor dynamics point of view, the motion induced forces acting to the impeller, cooling fan and seals should be negligible. The electric motor causes motion induced forces which might be of sufficient magnitude to have influence on rotor dynamics [1]. The tangential force caused by the motor has greatest destabilizing effect on the first forward bending mode when the speed is slightly above the bending critical speed. In the present case this effect adds approximately -0.5 % relative damping for the mode. In addition, the material damping on the rotor has a destabilizing effect on the first forward bending mode in the supercritical speed range. The position controller must provide enough damping for the first forward bending mode to compensate these destabilizing effects.

Maximum deceleration

The maximum deceleration of the motor occurs at frequency converter trip. The axial mass moment of inertia of the rotor is 0.135 kgm^2. At 250 kW output power and 320 Hz rotational speed this means deceleration rate of about 140 Hz/s. The torque, and thus the deceleration rate, is proportional to the square of the speed. The control system must be able to handle the unbalance response also in a rapid deceleration like this.

FEASIBLE SYNCHRONOUS RESPONSE

In this chapter an important force balance equation is derived and the bearing characteristics near the critical speed are analyzed, neglecting the stability considerations and details of the magnetic bearing. The position stiffness effect is also neglected since it has no practical effect on the results.

Force balance equation

Assuming a constant speed, isotropic bearing characteristics and neglecting all forces but bearing force and unbalance force, the signals behave as follows:

$$\boldsymbol{q}(\beta) = e^{i\beta}\boldsymbol{q}_{\text{s}},\ \boldsymbol{f}_{\text{B}}(\beta) = e^{i\beta}\boldsymbol{f}_{\text{Bs}},\ \boldsymbol{p}_{\text{S}}(\beta) = e^{i\beta}\boldsymbol{p}_{\text{Ss}} \qquad (2)$$

Subscript s refers to synchronous component of a signal. Steady state response can be solved from

$$\left[\boldsymbol{K}_{\text{rotor}} - \Omega^2\left(\boldsymbol{M}_{\text{rotor}} - \boldsymbol{G}_{\text{rotor}}\right)\right]\boldsymbol{q}_{\text{s}} = \boldsymbol{B}_{\text{B}}\boldsymbol{f}_{\text{Bs}} + \Omega^2\boldsymbol{U} \quad (3)$$

Speeds, where the coefficient matrix becomes singular are the free-free bending critical speeds and they can be solved from the following eigenvalue problem:

$$\boldsymbol{K}_{\text{rotor}}\boldsymbol{v}_n = \Omega_{crn}^2\left(\boldsymbol{M}_{\text{rotor}} - \boldsymbol{G}_{\text{rotor}}\right)\boldsymbol{v}_n \quad (4)$$

In this case, the first bending critical speed is Ω_{cr3}=207.5 Hz. The mode shape, $\boldsymbol{v}_3$, is scaled so that the displacement amplitudes over the whole rotor length are as close as possible to the amplitudes of the displacements of the mode shape of the non rotating rotor. The mode shape, $\boldsymbol{v}_3$, is plotted in Figure 2. The force balance equation is obtained by selecting $\Omega=\Omega_{\text{crn}}$ and multiplying Equation 3 from left by $\boldsymbol{v}_{\text{n}}$:

$$\boldsymbol{b}_n\boldsymbol{f}_{\text{Bs}} = -\Omega_{\text{crn}}^2 u_{crn} \quad (5)$$

where $\boldsymbol{b}_n = \boldsymbol{v}_n^{\text{T}}\boldsymbol{B}_{\text{B}} = \begin{bmatrix} b_{n1} & b_{n2} \end{bmatrix}$ and $u_{crn} = \boldsymbol{v}_n^{\text{T}}\boldsymbol{U}$. Exactly at the free-free bending critical speed a certain bearing force is needed to prevent the whirling amplitudes from growing to infinity. Thus, the free-free bending critical speeds are important in a fundamental manner. Naturally, also near the free-free bending critical speed bearing force is needed to limit the whirling amplitudes below an acceptable level.

At the critical speed the weighted sum of the synchronous bearing forces is determined by the modal unbalance, u_{crn}, according to Equation 5. To minimize the greater of the bearing forces it is necessary to adjust both forces equal in magnitude and in such phase that they both act against the unbalance force. In this way, the minimum bearing force needed to pass a bending critical speed, $F_{\text{Bmin}n}$, with a rotor having modal unbalance u_{crn} is obtained. We can also write the maximum tolerated modal unbalance, u_{crnmax}, as a function of the dynamic load capacity, F_{Bmax}:

$$\begin{aligned} F_{\text{B}\min n} &= \Omega_{\text{crn}}^2\left|u_{\text{crn}}\right| / \left(\left|b_{n1}\right| + \left|b_{n2}\right|\right) \\ u_{\text{crn}\max} &= \left(\left|b_{n1}\right| + \left|b_{n2}\right|\right) F_{\text{Bmax}}\left(\Omega_{\text{crn}}\right) / \Omega_{\text{crn}}^2 \end{aligned} \quad (6)$$

Assuming that the number of turns in the actuator is properly selected to utilize the full amplifier capability, the apparent power required from an amplifier of a bearing having dynamic load capacity of F_{Bmax} at frequency ω is [9]:

$$U_{\max} I_{\max} \approx 1.3 * F_{\text{Bmax}}\omega\delta \quad (7)$$

where δ is the air gap of the bearing, $U_{\max}$, is the available voltage and $I_{\max}$ is the maximum current of the amplifier.

In the present case, b_{31}=0.077, b_{32}=0.44 and the maximum bearing force at critical speed is about 800 N. This is sufficient to handle u_{cr3max}=246 gmm modal unbalance. The mode shape at the critical speed is so close to the mode shape at zero speed that u_{cr3} is practically the third element of vector $\boldsymbol{U}$ and vise versa. This is not generally true. The modal unbalance value, 246 gmm, is relatively high and with our rotor construction we expect our rotor unbalance to stay below it for the whole life time of the rotor. Obtaining 800 N force at 207 Hz requires about 750 VA amplifiers, which is half of the apparent power available.

Feasible bearing characteristics

It is not a trivial question, how to optimally use the bearing capability near the bending critical speed, when the strict force, displacement and other limitations are properly taken into consideration [10]. In the following, we do not aim for the optimum solution but rather for a feasible solution, so that the minimum dynamic load capacity requirement is not considerably increased because of poorly chosen bearing characteristics.

The bearing system measures the synchronous rotor vibration in the sensor locations, $\boldsymbol{p}_{\text{Ss}}$ and controls the synchronous bearing forces, $\boldsymbol{f}_{\text{Bs}}$. Because the controlled system (response from $\boldsymbol{f}_{\text{Bs}}$ to $\boldsymbol{p}_{\text{Ss}}$) is static and linear, we expect to find a feasible solution of the form

$$\boldsymbol{f}_{\text{Bs}} = -\boldsymbol{Z}\boldsymbol{p}_{\text{Ss}} \quad (8)$$

Our target is to find one constant feedback matrix, $\boldsymbol{Z}$, to be used in a wide speed range around the critical speed. Let us consider the optimum first. Write the equation of motion, Equation 3, in the following form:

$$\boldsymbol{p}_{\text{Ss}} = \boldsymbol{P}_{\text{Z}}\boldsymbol{f}_{\text{Bs}} + \boldsymbol{p}_{\text{Ss0}} = \boldsymbol{P}_{\text{Z}}\boldsymbol{f}_{\text{Bs}} + \boldsymbol{R}_{\text{Z}}\boldsymbol{U} \quad (9)$$

Define cost function

$$J\left(\Omega\right) = \text{E}\left(\boldsymbol{p}_{\text{Ss}}^{\text{H}}\boldsymbol{W}_{\text{P}}\boldsymbol{p}_{\text{Ss}} + \boldsymbol{f}_{\text{Bs}}^{\text{H}}\boldsymbol{W}_{\text{F}}\boldsymbol{f}_{\text{Bs}}\right) \quad (10)$$

where E denotes expectation value and $\boldsymbol{W}_{\text{P}}$ and $\boldsymbol{W}_{\text{F}}$ are weight matrices. Let us also define $\text{E}(\boldsymbol{U}\boldsymbol{U}^{\text{H}})=\boldsymbol{W}_{\text{U}}$. Cost function, Equation 10, is not the most accurate description of the actual requirements, see [10], but it is mathematically easy to handle and serves our purposes well enough. The synchronous force that minimizes the cost function can be expressed in feedback form, Equation 8, and the optimum **Z**-matrix is:

$$\boldsymbol{Z}_{\text{opt}}\left(\Omega\right) = \boldsymbol{W}_{\text{F}}^{-1}\boldsymbol{P}_{\text{Z}}^{\text{H}}\left(\Omega\right)\boldsymbol{W}_{\text{P}} \quad (11)$$

$\boldsymbol{Z}_{\mathrm{opt}}$ is a real valued speed-dependent feedback matrix. It is interesting to note that the optimum feedback matrix does not depend on $\boldsymbol{W}_{\mathrm{U}}$. Naturally, the optimum value of the cost function, J_{opt}, depends on $\boldsymbol{W}_{\mathrm{U}}$.

Let us denote by $J(\Omega,\boldsymbol{Z})$ the value of the cost function when the bearing force is produced by feedback, Equation 8.

$$J\left(\Omega,\boldsymbol{Z}\right)=\mathrm{trace}\left[\boldsymbol{W}_{\mathrm{U}}\boldsymbol{R}_{\mathrm{Z}}^{\mathrm{H}}\boldsymbol{S}_{\mathrm{Z}}^{\mathrm{H}}\left(\boldsymbol{W}_{\mathrm{P}}+\boldsymbol{Z}^{\mathrm{H}}\boldsymbol{W}_{\mathrm{F}}\boldsymbol{Z}\right)\boldsymbol{S}_{\mathrm{Z}}\boldsymbol{R}_{\mathrm{Z}}\right] \quad (12)$$

where $\boldsymbol{S}_{\mathrm{Z}}=(\boldsymbol{I}+\boldsymbol{P}_{\mathrm{Z}}\boldsymbol{Z})^{-1}$. When passing the critical speed it is not necessary to minimize J for every speed. It is enough to keep the maximum value of $J(\Omega,\boldsymbol{Z})$ in an acceptable level, i.e. so that it does not significantly exceed the maximum value of J_{opt} over the speed range of interest. Let us denote maximum of J_{opt} over the speed range of interest by J_{ref}. When searching the best constant $\boldsymbol{Z}$, speed range from 160 Hz to 260 Hz was selected. The position weight was $W_{\mathrm{P}}=1/(100\mu\mathrm{m})^2$. The force weight was $W_{\mathrm{F}}=1/(800\mathrm{N})^2$ up to 207 Hz and increased relative to second power of speed above that and the unbalance weight was $\boldsymbol{W}_{\mathrm{U}}=\mathrm{diag}(|\boldsymbol{U}_{\mathrm{tst}}|)^2$. Equally distributed speeds, Ω_{k}, were defined with 5 Hz step. Then $\boldsymbol{Z}$ minimizing the maximum of $J(\Omega_{\mathrm{k}},\boldsymbol{Z})$ was numerically determined. Two solutions, $\boldsymbol{Z}_{\mathrm{A}}$ and $\boldsymbol{Z}_{\mathrm{B}}$ were obtained. After rounding:

$$\boldsymbol{Z}_{\mathrm{A}}=-i\begin{bmatrix}0 & 2\\ 4 & 10\end{bmatrix}\mathrm{MN/m},\quad \boldsymbol{Z}_{\mathrm{B}}=-\boldsymbol{Z}_{\mathrm{A}} \quad (13)$$

The machine rotates to the negative direction around the Z-axis, i.e. Ω is negative. The solution $\boldsymbol{Z}_{\mathrm{A}}$ is a natural kind of a solution where the bearing force is to the opposite direction of synchronous whirling motion. In the solution B, the bearing force is to the same direction as the rotor moves. So, we have negative damping in the bearings. Note that the solution minimizing the defined criterion depends on $\boldsymbol{W}_{\mathrm{U}}$.

In Figure 4 $J(\Omega_{\mathrm{k}},\boldsymbol{Z})$ with $\boldsymbol{Z}_{\mathrm{opt}}$, $\boldsymbol{Z}_{\mathrm{A/B}}$, $\boldsymbol{Z}=\boldsymbol{0}$, $\boldsymbol{Z}_{\mathrm{wc}}=\infty\boldsymbol{I}$ and $\boldsymbol{Z}_{\mathrm{wc2}}$ are shown. $\boldsymbol{Z}_{\mathrm{wc2}}$ means whirling cancellation only in end 2. As can be seen, the maximum of $J(\Omega,\boldsymbol{Z}_{\mathrm{A/B}})$ over the speed range is not much greater than J_{ref}. The whirling cancellation in only end 2 works well near the critical speed but the solutions $\boldsymbol{Z}_{\mathrm{A/B}}$ work across a wider speed range. Whirling cancellation in both ends leads to great bearing forces in end 1 due to rigid body unbalance. Far away from the critical speed the force cancellation approaches the optimum solution.

In Figure 5 the unbalance responses are plotted for solutions $\boldsymbol{Z}_{\mathrm{A}}$, $\boldsymbol{Z}_{\mathrm{B}}$ and $\boldsymbol{Z}=\boldsymbol{0}$.

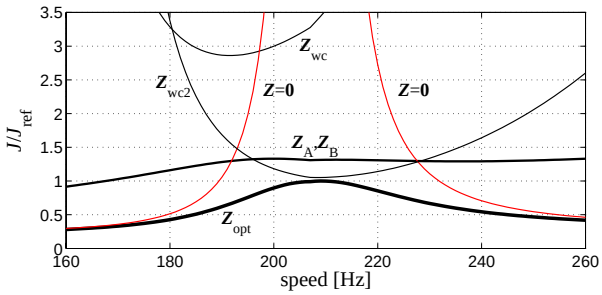

FIGURE 4: $J(\Omega,Z)/J_{\mathrm{ref}}$ for different options.

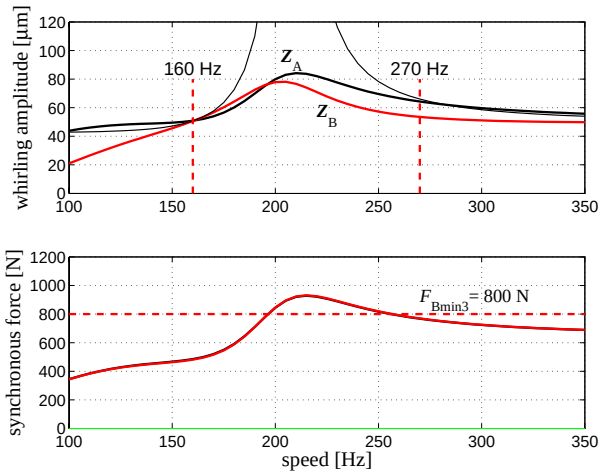

FIGURE 5: Unbalance response with $\boldsymbol{Z}=\boldsymbol{Z}_{\mathrm{A}}$, $\boldsymbol{Z}=\boldsymbol{Z}_{\mathrm{B}}$ and $\boldsymbol{Z}=\boldsymbol{0}$ (thin curve). The curves are from the 2-end.

Both $\boldsymbol{Z}_{\mathrm{A}}$ and $\boldsymbol{Z}_{\mathrm{B}}$ work equally well near the critical speed. With $\boldsymbol{U}_{\mathrm{tst}}$ the whirling radii remain in an acceptable level and the maximum bearing force exceeds F_{Bmin3} only slightly. Comparing to the responses with $\boldsymbol{Z}=0$, we choose that $\boldsymbol{Z}=\boldsymbol{Z}_{\mathrm{A/B}}$ should be used in the speed range from 160 Hz to 270 Hz. Above 270 Hz the force cancellation strategy, ($\boldsymbol{Z}=0$) is used in order to reduce the loading of the power electronics. $\boldsymbol{Z}=0$ can be used with speeds below 160 Hz, if necessary.

CONTROL SYSTEM SYNTHESIS

The control system is shown in Figure 6. Complex formulation is extensively used in the controller synthesis. Position $\boldsymbol{p}$, displacement $\boldsymbol{d}$ and control current $\boldsymbol{J}$ are complex vectors with two elements, where the first element is the signal in the 1-end and the second in the 2-end.

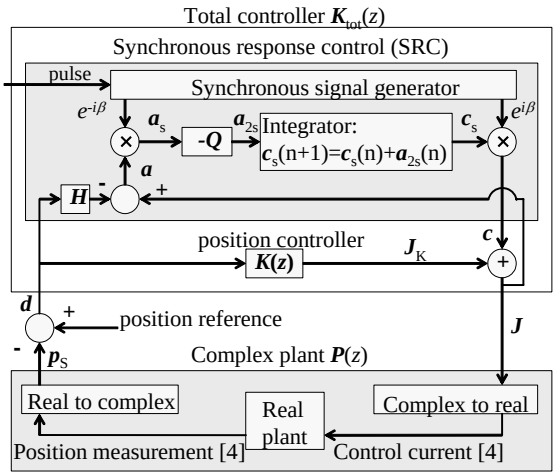

FIGURE 6: The control system.

If we assume isotropic bearing characteristics and neglect the stator side mechanics, the plant $\boldsymbol{P}$ will be isotropic and its dynamics can be written as:

$$\begin{aligned}\boldsymbol{x}_{\mathrm{P}}(n+1) &= \boldsymbol{A}_{\mathrm{P}}\boldsymbol{x}_{\mathrm{P}}(n) + \boldsymbol{B}_{\mathrm{PJ}}\boldsymbol{J}(n) + \Omega^2 e^{i\beta}\boldsymbol{B}_{\mathrm{PU}}\boldsymbol{U} \\ \boldsymbol{p}_{\mathrm{S}}(n) &= \boldsymbol{C}_{\mathrm{P}}\boldsymbol{x}_{\mathrm{P}}(n)\end{aligned} \tag{14}$$

The process dynamics depend on the rotational speed due to gyroscopic coupling.

The controller consists of a position controller, $\boldsymbol{K}$, and SRC in parallel with it. Together they constitute the total controller, $\boldsymbol{K}_{\mathrm{tot}}$. After some straightforward mathematics the total controller can be expressed in the following state space form:

$$\begin{aligned}\begin{bmatrix}\boldsymbol{x}_{\mathrm{K}}(n+1)\\ \boldsymbol{c}(n+1)\end{bmatrix} &= \begin{bmatrix}\boldsymbol{A}_{\mathrm{K}} & \boldsymbol{0}\\ -e^{i\Omega T}\boldsymbol{Q}\boldsymbol{C}_{\mathrm{K}} & e^{i\Omega T}(\boldsymbol{I}-\boldsymbol{Q})\end{bmatrix}\begin{bmatrix}\boldsymbol{x}_{\mathrm{K}}(n)\\ \boldsymbol{c}(n)\end{bmatrix} + \\ &\quad \begin{bmatrix}\boldsymbol{B}_{\mathrm{K}}\\ e^{i\Omega T}\boldsymbol{Q}(\boldsymbol{H}-\boldsymbol{D}_{\mathrm{K}})\end{bmatrix}\boldsymbol{d}(n) \\ \boldsymbol{J}(n) &= \begin{bmatrix}\boldsymbol{C}_{\mathrm{K}} & \boldsymbol{I}\end{bmatrix}\begin{bmatrix}\boldsymbol{x}_{\mathrm{K}}(n)\\ \boldsymbol{c}(n)\end{bmatrix} + \boldsymbol{D}_{\mathrm{K}}\boldsymbol{d}(n)\end{aligned} \tag{15}$$

where $\boldsymbol{A}_{\mathrm{K}}$, $\boldsymbol{B}_{\mathrm{K}}$, $\boldsymbol{C}_{\mathrm{K}}$ and $\boldsymbol{D}_{\mathrm{K}}$ are the matrices of the state space presentation of $\boldsymbol{K}$. At a constant speed, the total controller behaves as a linear time invariant system. It is also straightforward to show that the synchronous response of the total controller is $\boldsymbol{K}_{\mathrm{tot}}(e^{i\Omega T})=\boldsymbol{H}$. Value of the $\boldsymbol{H}$-matrix is obtained from the $\boldsymbol{Z}$-matrix by compensating the control delays and amplifier dynamics:

$$\boldsymbol{H} = \frac{1}{k_{\mathrm{I}}\, g(i\Omega_{\mathrm{cr3}})}\boldsymbol{Z} \tag{16}$$

Synthesis of the position controller

In the design of the position controller the emphasis is not on the unbalance response. Main target is to guarantee stability in the whole speed range with all parameter variations. In addition, low frequency stiffness and damping and high frequency gain need to be considered.

The position controller was synthesized using the frequency domain approach presented in [9]. Frequency domain design methods have the advantage that the effects of the design changes on the performance and robustness are easy to see. The controller consists of constant real input and output transformation matrices, $\boldsymbol{R}_1$ and $\boldsymbol{R}_2$, respectively and a diagonal controller between them. See Figure 7.

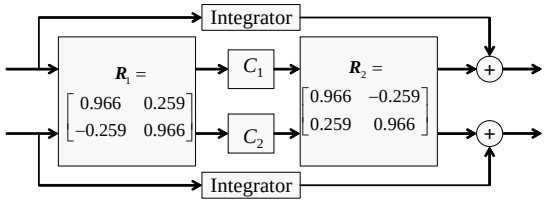

FIGURE 7: Structure of the position controller.

In the case of a subcritical machine, where the bending modes are clearly above the position control loop gain crossover frequency, this approach is well justified and the selection of the transformation matrices is straightforward. In the present case, we started by selecting the optimal transformation matrices for a rigid rotor [9]. Then the matrices were slightly adjusted so that the polarity in which the bending modes are visible for the controllers C_1 and C_2 does not change when the actuator gain and sensor sensitivities vary in their expected range. The polarity of the three first bending modes is the same for all modes and both of the controllers.

The frequency responses for the process seen by controllers C_1 and C_2 (when other controller is open) were computed for zero speed, maximum speed and one speed in between them. Controllers C_1 and C_2 were designed using graphical SISO design tool, which provides effective means of manipulating the shape of the open loop frequency response. The frequency responses of the controllers are shown in Figure 8. The position controller has a total of 21 complex states.

The frequency response of the obtained position controller is quite different from $\boldsymbol{H}_{\mathrm{A/B}}$. Especially, we were not able to obtain sufficient phase lead in the vicinity of the critical speed. As a consequence, the unbalance response is unacceptable as shown in Figure 9. The maximum tolerated modal unbalance is only 35 gmm. From Figure 9 it can be seen that below 160 Hz the position controller gives satisfactory response and no SRC is needed.

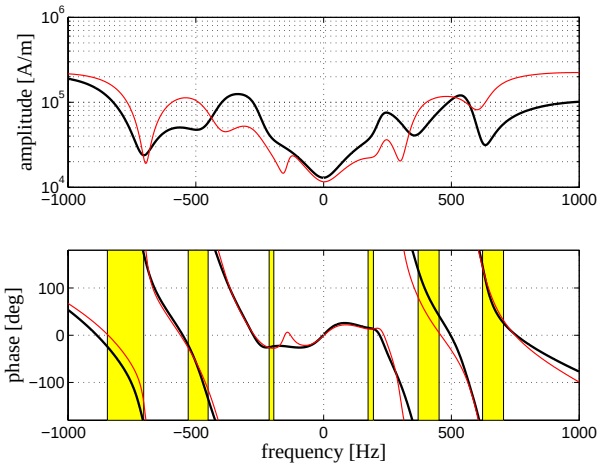

FIGURE 8: Frequency responses of gC_1 (bold curve) and gC_2 (thin curve). The shaded areas in the phase plot indicate the range where the free-free natural frequency of a bending mode changes as the speed varies between 0 Hz and 400 Hz.

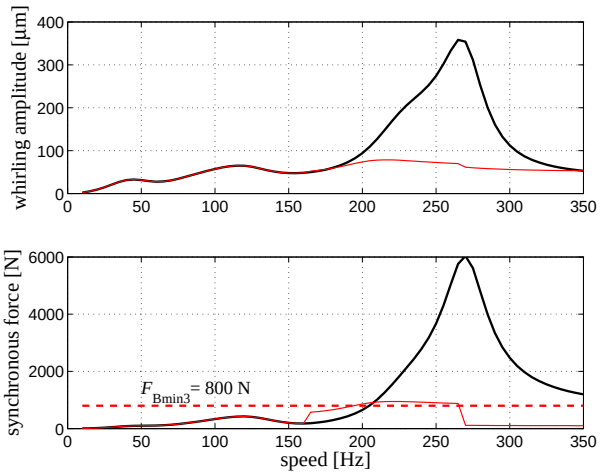

FIGURE 9: Steady state unbalance response in the 2-end without SRC (bold curve) and with SRC (thin curve).

Design of the position controller was a challenging task: the first five bending modes had to be considered and the second and the third modes were relatively gyroscopic. In fact, the stability margins obtained with the designed controller are not sufficient for series production. We did not implement a speed scheduled position controller, but that would have solved the problem.

Determination of Q-matrices

Pulse transfer function from signal $\boldsymbol{c}$ to $\boldsymbol{a}$ is

$$\boldsymbol{S}_{\mathrm{H}}(z)=\left(\boldsymbol{I}+\boldsymbol{H}\boldsymbol{P}(z)\right)\left(\boldsymbol{I}+\boldsymbol{K}(z)\boldsymbol{P}(z)\right)^{-1} \qquad (17)$$

Assuming that the system $\boldsymbol{S}_{\mathrm{H}}$ is clearly faster than the convergence rate of SRC, we can write the following approximate differential equation for $\boldsymbol{a}_{\mathrm{s}}$:

$$\frac{d\boldsymbol{a}_{\mathrm{s}}}{dt}=-\frac{1}{T}\boldsymbol{S}_{\mathrm{H}}\left(e^{i\Omega T}\right)\boldsymbol{Q}\boldsymbol{a}_{\mathrm{s}}=\boldsymbol{A}_{\mathrm{H}}\boldsymbol{a}_{\mathrm{s}} \qquad (18)$$

In order to obtain a convergent system, the eigenvalues of $\boldsymbol{A}_{\mathrm{H}}$ must be on the left half plane. Absolute value of $\boldsymbol{Q}$-matrix is scaled so that the convergence rate is sufficiently low to avoid stability problems but fast enough for SRC to keep the bearing forces near the steady state values also in the fast deceleration of the compressor. Problem of selecting $\boldsymbol{Q}$ has been studied by several authors [2], [7] and [9].

We used the obvious approach: The speed range where SRC is used was divided into small number of intervals. For every interval $\boldsymbol{S}_{\mathrm{Hmid}}$ was determined at a speed near the middle of the interval and a constant $\boldsymbol{Q}$ for the interval was selected as

$$\boldsymbol{Q}=\frac{T}{\tau}\boldsymbol{S}_{\mathrm{Hmid}}^{-1} \qquad (19)$$

where τ is the desired time constant. The speed range of 270 Hz to 320 Hz ($\boldsymbol{H}=\boldsymbol{0}$) was divided into two scheduling intervals and time constant 0.125 s was used because of the fast deceleration rate at high speed. The speed range from 160 Hz to 270 Hz was divided into two scheduling intervals in SCR A. In SRC B, the same speed range had to be divided into four intervals. With SRC A the total controller was stable at every interval, whereas with SRC B the total controller was unstable in two first scheduling intervals. Time constant for range 160 Hz to 270 Hz was 0.5 s, because the deceleration rate is lower there.

The stability of SRC was analyzed using numerical range. Numerical range of a square matrix $\boldsymbol{X}$ is a set of complex numbers defined as follows:

$$\varphi(\boldsymbol{X})=\left\{\boldsymbol{x}^{\mathrm{H}}\boldsymbol{X}\boldsymbol{x}\,\middle|\,\boldsymbol{x}\in\mathrm{C}^{N\times 1},\boldsymbol{x}^{\mathrm{H}}\boldsymbol{x}=1\right\} \qquad (20)$$

Numerical range is a convex region in complex plane and it includes the eigenvalues of the matrix.

Using numerical range is preferred to computing eigenvalues, since in addition to stability, numerical range in the left half plane implies a steady convergence in the following sense:

$$\begin{aligned}&\frac{d}{dt}f=2\,\mathrm{Real}\left(\boldsymbol{a}_{\mathrm{s}}^{\mathrm{H}}\boldsymbol{A}_{\mathrm{H}}\boldsymbol{a}_{\mathrm{s}}\right)<2\max\left[\mathrm{real}\,\varphi\left(\boldsymbol{A}_{\mathrm{H}}\right)\right]f\\&f=\boldsymbol{a}_{\mathrm{s}}^{\mathrm{H}}\boldsymbol{a}_{\mathrm{s}}\end{aligned} \qquad (21)$$

Thus, if the whole numerical range $\varphi(\boldsymbol{A}_{\mathrm{H}})$ is clearly on the left half plane we can expect smooth behavior in transient situations and when starting the algorithm.

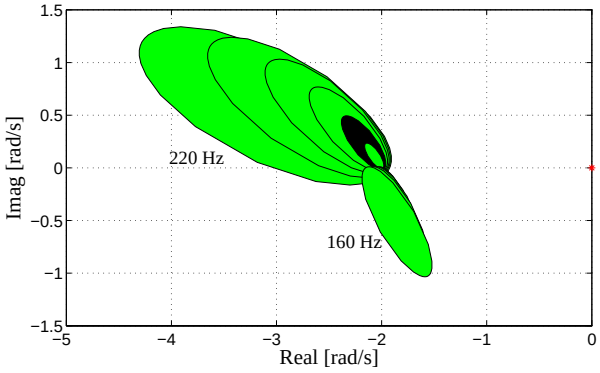

FIGURE 10: Numerical ranges of $\boldsymbol{A}_{\mathrm{H}}$ for speeds 160 Hz, 165 Hz,...,220 Hz. For $\boldsymbol{H}=\boldsymbol{H}_{\mathrm{A}}$ and $\boldsymbol{Q}$ computed at 190 Hz.

Simulated unbalance responses

Figure 11 shows the steady state unbalance response and transient unbalance response as the compressor is decelerating freely. As can be seen, both SRC options give good results. In fast deceleration neither SRC manages to keep the signals close to the steady state values. However, responses stay in an acceptable level with both options.

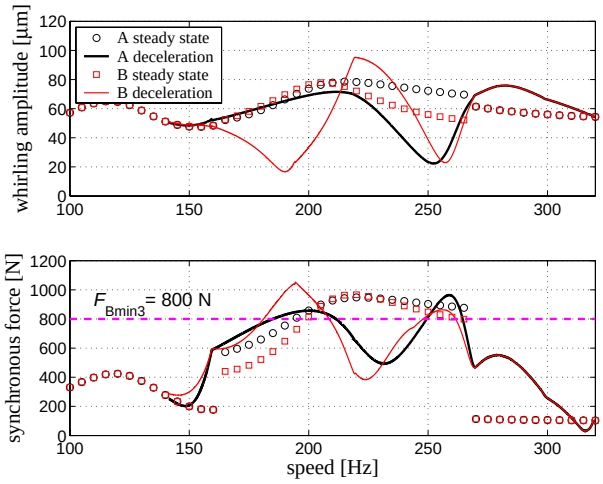

FIGURE 11: Unbalance response using SRC A and SRC B in steady state and when decelerating freely. Responses are the amplitudes in the 2-end bearing.

MEASUREMENTS

The tests were done with the prototype compressor. The motor was accelerated slowly up to the maximum speed, 320 Hz, and decelerated back to zero. As the first bending mode is better seen in end 2 of the motor, we only present the measured signals and responses in that end. We unbalanced the rotor so that the modal unbalance of the first bending mode was approximately 110 gmm. The measured amplitudes of the rotational synchronous components over the speed range of interest are shown in Figure 12:

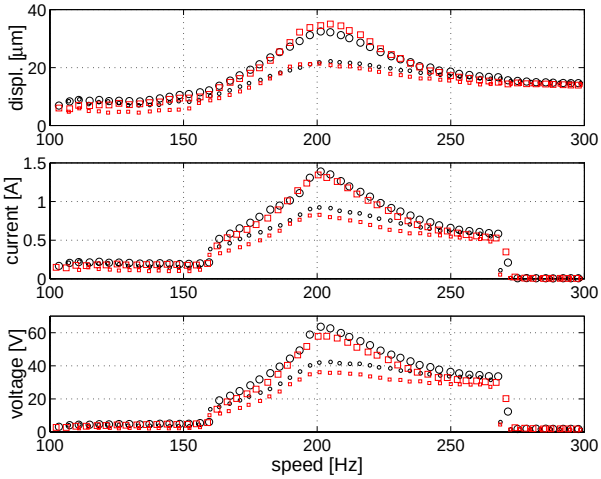

FIGURE 12: The measured amplitudes of synchronous components of displacement, coil current and coil voltage in the radial bearing in end 2 of the motor as a function of rotational speed. The circles are measured for SRC A and the squares for SRC B. The larger markers are for acceleration and the smaller for deceleration slopes.

Below 160 Hz there is no unbalance compensation. Between frequencies 160 Hz and 270 Hz both SRC A and SRC B strategies seem to work equally well as the simulation predicted. Above 270 Hz the force cancellation strategy effectively removes the synchronous currents.

There is a clear difference in the responses between the acceleration and deceleration curves. This was due to mechanical changes in the rotor caused by either thermal effects or centrifugal stresses.

The rotational synchronous position components, S_{X} and S_{Y} for X- and Y-channels respectively, were calculated from the position measurements, p_{mX} and p_{mY}, as $S_{\mathrm{X/Y}}=2*\mathrm{LPF}(p_{\mathrm{mX/Y}}e^{-i\left|\beta_{\mathrm{m}}\right|})$, where β_{m} is the measured rotational angle with respect to the positive X-axis and LPF stands for low pass filtering. For $\Omega<0$ the complex formulated position in rotating coordinates, $\boldsymbol{p}_{\mathrm{R}}$, is:

$$\boldsymbol{p}_{\mathrm{R}} = e^{-i\beta}\boldsymbol{p} = \frac{S_{\mathrm{X}}^{*}}{2} + i\frac{S_{\mathrm{Y}}^{*}}{2} + e^{-i2\beta}\left(\frac{S_{\mathrm{X}}}{2} + i\frac{S_{\mathrm{Y}}}{2}\right) \qquad (22)$$
$$= \boldsymbol{p}_{\mathrm{R0}} + e^{-i2\beta}\boldsymbol{p}_{\mathrm{RW}}$$

where $\boldsymbol{p}_{\mathrm{R0}}$ is the average position of the rotor in the rotating coordinate system. For circular whirling orbit $\boldsymbol{p}_{\mathrm{RW}}$ becomes zero and the position does not depend on rotational angle, β. Due to anisotropy in the stator side, the whirling orbit of the rotor becomes elliptic. This is

seen as a circular whirling at frequency 2Ω in the rotating coordinate system. This whirling is described by $\boldsymbol{p}_{\mathrm{RW}}$ in Equation 22. The measured rotor positions are shown in Figure 13.

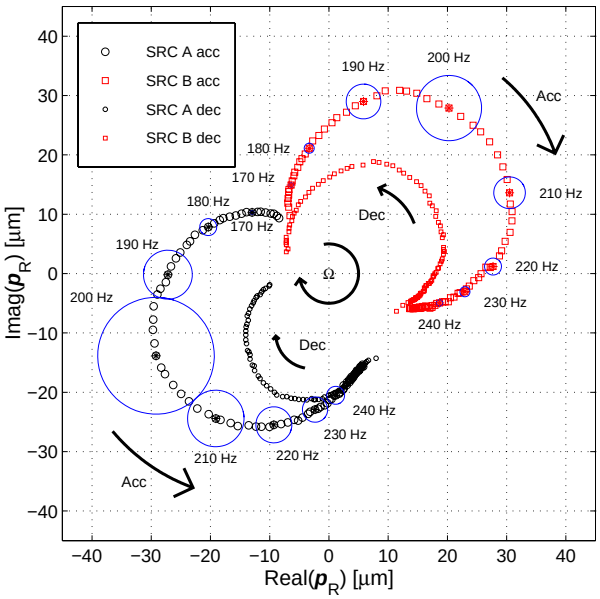

FIGURE 13: The measured position of the center point of the rotor in rotating coordinates in the sensor plane of end 2 of the rotor on the speed range from 160 Hz to 270 Hz. The direction of the change of position when accelerating (Acc) and decelerating (Dec) is shown. The average positions, $\boldsymbol{p}_{\mathrm{R0}}$, are shown with circles (SRC A) and squares (SRC B). Speeds 170,180 … 240 Hz on acceleration curves are highlighted with asterisks and a circle with a radius of the rotor coordinate whirling amplitude $|\boldsymbol{p}_{\mathrm{RW}}|$ is shown around them. Direction of rotation, Ω, is shown.

CONCLUSIONS

AMB control system design of a supercritical turbo compressor was successfully carried out and validated by the measurements with an actual machine. Determining the physical boundary conditions and design of the synchronous response control was straightforward. The position controller design, however, was a challenging task because the first five of the bending modes had to be considered and especially since the second and the third modes were relatively gyroscopic. Covering the whole speed range with one constant parameter controller turned out to be difficult in this case. An interesting fact is that, from the unbalance response point of view, the synchronous bearing force near the critical speed may as well be to the same direction as to the opposite direction of the rotor motion. In the present case the former option, the negative damping solution, however, led to unstable total controller and smaller stability margins compared to the latter choice.

REFERENCES

1. Arkkio A., Antila M., Pokki K., Simon A., Lantto E., Electromagnetic Force on a Whirling Cage Rotor, IEEE Proceedings-Electric Power Applications, Vol. 147, pp.353-360, 2000.
2. Betschon F., Knospe C., Reducing Magnetic Bearing Currents Via Gain Scheduled Adaptive Control, IEEE/ASME Transactions on Mechatronics, Vol. 6, NO. 4, 2001.
3. Genta G., Dynamics of Rotating Systems, ISBN 0-387-20936-0, Springer, 2005.
4. Haberman, H., Brunet, M. Joly P., Device for Compensating Synchronous Disturbances in the Magnetic Suspension of a Rotor, US patent 4,121,143, 1978.
5. Haberman, H., Brunet, M., Device for Damping the Critical Frequencies of a Rotor Suspended by a radial Electromagnetic Bearing, US patent 4,128,795, 1978.
6. Haberman, H., Brunet, M., The Active Magnetic Bearing Enables Optimum Damping of Flexible Rotors, International Journal of Turbo and Jet Engines 3, pp. 63-77, 1986.
7. Herzog, R., Buhler, P., Gähler C., Larsonneur R., Unbalance Compensation Using Generalized Notch Filters in the Multivariable Feedback of Magnetic Bearings, IEEE Transactions on Control Systems Technology, 4, No. 5, pp. 580-586, 1996.
8. Knospe C, Tamer S, Fedigan S., Robustness of Adaptive Rotor Vibration Control to Structured Uncertainty, Journal of Dynamic Systems, Measurement and Control, Vol. 119, pp. 243-250, 1997.
9. Lantto E., Robust Control of Magnetic Bearings in Subcritical Machines, Acta Polytechnica Scandinavica, Electrical Engineering Series No. 94, ISBN 952-5148-80-7, Espoo, Finland, 1999.
10. Maslen E., Allaire P., Magnetic Bearing Sizing for Flexible Rotors, Journal of Tribology, Vol. 114, pp. 223-229, 1992.

APPENDIX A: The values of rotor model matrices

$$\boldsymbol{M}_{\mathrm{rotor}} = \mathrm{diag}\left(\begin{bmatrix} 62.98 & 5.10 & 8.85 & 4.81 & 7.80 & 9.69 & 7.17 \end{bmatrix}\right)$$

$$\boldsymbol{G}_{\mathrm{rotor}} = \begin{bmatrix} 0 & 0 & 0 & 0 & 0 & 0 & 0 \\ 0 & 0.135 & 0.141 & 0.315 & 0.478 & -0.302 & -0.120 \\ 0 & 0.141 & 1.109 & 1.224 & 1.756 & -0.695 & 0.958 \\ 0 & 0.315 & 1.224 & 2.577 & 2.596 & -2.143 & 1.181 \\ 0 & 0.478 & 1.756 & 2.596 & 5.316 & -2.402 & 1.196 \\ 0 & -0.302 & -0.695 & -2.143 & -2.402 & 2.978 & -0.574 \\ 0 & -0.120 & 0.958 & 1.181 & 1.196 & -0.574 & 2.275 \end{bmatrix}$$

$$\boldsymbol{K}_{\mathrm{rotor}} = \mathrm{diag}\left(\begin{bmatrix} 0 & 0 & 0.133 & 0.388 & 1.53 & 7.05 & 9.56 \end{bmatrix}\right) * 10^{8}$$

$$\boldsymbol{B}_{\mathrm{S}} = \begin{bmatrix} 1 & 0.361 & 0.235 & -0.178 & -0.390 & 0.161 & 0.032 \\ 1 & -0.472 & 0.644 & -0.352 & 0.366 & 0.383 & 0.276 \end{bmatrix}^{\mathrm{T}}$$

$$\boldsymbol{B}_{\mathrm{B}} = \begin{bmatrix} 1 & 0.300 & 0.051 & -0.271 & -0.200 & -0.267 & 0.337 \\ 1 & -0.411 & 0.444 & -0.146 & 0.063 & -0.108 & -0.211 \end{bmatrix}^{\mathrm{T}}$$

$$\boldsymbol{U}_{\mathrm{tst}} = \begin{bmatrix} 1414 - 1414i & 212 + 212i & 239 & 0 & 0 & 0 & 0 \end{bmatrix}^{\mathrm{T}} 10^{-6}$$